AGU PUBLICATIONS

Geophysical Research Letters

RESEARCH LETTER
10.1002/2016GL068436

Key Points:
- Localized regions of elevated geothermal heat flux may organize ice flow in regions of relatively slow ice flow
- Fast-flowing glaciers are unaffected by localized elevated geothermal heat flux
- Improved estimates of fine-scale geothermal heat flux are needed to assess possible impacts on ice dynamics and mass budget estimates

Supporting Information:
- Supporting Information S1
- Figure S1

Correspondence to:
M. L. Pittard,
mark.pittard@utas.edu.au

Citation:
Pittard, M. L., B. K. Galton-Fenzi, J. L. Roberts, and C. S. Watson (2016), Organization of ice flow by localized regions of elevated geothermal heat flux, *Geophys. Res. Lett.*, *43*, 3342–3350, doi:10.1002/2016GL068436.

Received 29 FEB 2016
Accepted 16 MAR 2016
Accepted article online 21 Mar 2016
Published online 6 APR 2016

Organization of ice flow by localized regions of elevated geothermal heat flux

M. L. Pittard[1,2], B. K. Galton-Fenzi[2,3], J. L. Roberts[2,3], and C. S. Watson[4]

[1]Institute for Marine and Antarctic Studies, University of Tasmania, Hobart, Tasmania, Australia, [2]Antarctic Climate & Ecosystems Cooperative Research Centre, University of Tasmania, Hobart, Tasmania, Australia, [3]Australian Antarctic Division, Kingston, Tasmania, Australia, [4]School of Land and Food, University of Tasmania, Hobart, Tasmania, Australia

Abstract The impact of localized regions of elevated geothermal heat flux on ice sheet dynamics is largely unknown. Simulations of ice dynamics are produced using poorly resolved and low-resolution estimates of geothermal heat flux. Observations of crustal heat production within the continental crust underneath the Lambert-Amery glacial system in East Antarctica indicate that high heat flux regions of at least 120 mW m^{-2} exist. Here we investigate the influence of simulated but plausible, localized regions of elevated geothermal heat flux on ice dynamics using a numerical ice sheet model of the Lambert-Amery glacial system. We find that high heat flux regions have a significant effect across areas of slow-moving ice with the influence extending both upstream and downstream of the geothermal anomaly, while fast-moving ice is relatively unaffected. Our results suggest that localized regions of elevated geothermal heat flux may play an important role in the organization of ice sheet flow.

1. Introduction

Geothermal heat flux (GHF) has an important control on ice dynamics and contributes to the temperature distribution of the ice and influences ice flow by varying ice viscosity and basal lubrication. The magnitude of the GHF depends on spatially varying geological conditions that control heat production and conduction such as the mantle heat flux, crustal thickness, local radiogenic crustal heat production (RCHP), and groundwater flow [*Sandiford and McLaren*, 2002; *Fox Maule et al.*, 2005; *Carson et al.*, 2014; *Gooch et al.*, 2016]. GHF is difficult to directly measure under the Antarctica Ice Sheet due to limited access to the bedrock, with only a few point measurements in ice-free areas or from borehole sampling [*Fisher et al.*, 2015]. The lack of direct measurements led to the development of model-based methods that infer GHF from seismic [*Shapiro and Ritzwoller*, 2004] and magnetic field [*Fox Maule et al.*, 2005] models. *Shapiro and Ritzwoller* [2004] created a global seismic model of the crust and upper mantle based on known GHF observations then extrapolated it to regions where observations were rare or absent. The resulting GHF data set has a coarse resolution (600 km) and does not reflect fine-scale spatial variability in GHF caused by RCHP. *Fox Maule et al.* [2005] use satellite magnetic data to calculate GHF by estimating the depth to the Curie temperature (the depth where the magnetic properties of rocks are still dependant on temperature) and then constructing a thermal model assuming various thermal properties including the placements of the Curie isotherm at the lower boundary of the magnetic crust. The resulting GHF data set is limited in resolution to a few hundred kilometers, yet it is known that GHF can vary by a factor of at least 2 on scale of tens of kilometers as a result of geological settings such as RCHP [*Carson and Pittard*, 2012; *Carson et al.*, 2014] and groundwater [*Gooch et al.*, 2016]. A direct measurement of the GHF at a subglacial lake in West Antarctica found that the GHF was highly elevated at 285 mW m^{-2}, compared to the calculated background field from remote sensing of approximately 115–150 mW m^{-2} [*Fisher et al.*, 2015].

Geochemical analysis of exposed rocks in the Prydz Bay region observed high RCHP which may be present in the inland regions [*Carson et al.*, 2014]. During a number of expeditions in this region, rock samples were taken and later analyzed for heat-producing elements (Th, Ur, and K) to determine crustal heat production [*Carson and Pittard*, 2012]. The heat-producing elements are preferentially found in the upper 10–15 km of crust and can contribute over 50% of the total surface heat flow [*Sandiford and McLaren*, 2002]. A standard granite with a heat production value of 2.5 μW m^{-3} is typical of regions with a surface heat flow of approximately 60 mW m^{-2} [*Sandiford and McLaren*, 2002], while outcrops of Cambrian granites measured in the Prydz Bay region had heat production values of 3.75 to 65.85 μW m^{-3} [*Carson and Pittard*, 2012], which 2-D modeling of the region estimated that the surface heat flow could be 80–90 mW^{-2}, with peak values of at

least 120 mW m^{-2} [*Carson et al.*, 2014]. Groundwater flow toward the base of the ice could also contribute to elevated geothermal heat flux, with estimates of the contribution within East Antarctica from groundwater flow of up to 24–28.8 mW m^{-2} [*Gooch et al.*, 2016]. An updated GHF regional map based on the M7 magnetic model [*Fox Maule et al.*, 2005] agrees well with *Carson et al.* [2014] showing elevated GHF in the Prydz Bay region with values up to 150 mW m^{-2}, albeit primarily offshore. The updated seismic-derived GHF from *An et al.* [2015] shows elevated GHF at 70–80 mW m^{-2} in a similar region; however, this method uses a regionally constant RCHP and hence would not reflect any spatial variations in GHF due to RCHP. Both these data sets do not capture the local fine-scale variations in GHF from local crustal heat production or possible groundwater flow.

The East Antarctic Ice Sheet likely has heterogeneous subglacial heat flow due to the spatial variability of high heat-producing granites in the upper crust [*Carson et al.*, 2014] and possibly groundwater flow [*Gooch et al.*, 2016]. *Carson et al.* [2014] highlight that further quantifying the subglacial heat flow would require the delineation of the location and distribution of these Cambrian aged orogenic terraces under the ice sheet, while *Gooch et al.* [2016] suggest that groundwater volume flux rates will increase local geothermal heat flux across sedimentary basins and in discrete locations such as fault zones. Given the prohibitive logistical constraints to directly measure the subglacial conditions, we investigate how these heat-producing regions, if they extended inland underneath the Lambert-Amery glacial system, would influence ice sheet flow within a numerical model of the region. We insert simulated, but likely realistic, high heat flux regions (HHFR) into the background GHF of different regions that characterize different flow regimes and investigate the influence elevated geothermal heat flux has on modeled ice sheet flow.

2. Lambert-Amery Glacial System Regional Model

The Lambert-Amery glacial system is located in East Antarctica (Figure 1). It has been shown to be relatively stable under present conditions [*King et al.*, 2007; *Yu et al.*, 2010; *Wen et al.*, 2010; *King et al.*, 2012; *Pittard et al.*, 2015] yet is a region which is often poorly represented in Antarctic Ice Sheet models due to large regions that lack topographic measurements [*Fretwell et al.*, 2013] and difficulties in stabilizing the grounding line in its present location [*Martin et al.*, 2011; *Golledge et al.*, 2012].

The model used for this study is the Parallel Ice Sheet Model (PISM) version 0.6.2 [*Bueler et al.*, 2007; *Bueler and Brown*, 2009; *Winkelmann et al.*, 2011]. PISM is a three-dimensional thermodynamically coupled model with a shallow ice approximation (SIA) and shallow shelf approximation (SSA) hybrid scheme that utilizes a structured finite difference discretization. The SIA approximates ice flow for grounded ice where vertical shear dominates, and the SSA approximates ice flow for floating ice where horizontal shear dominates. In grounded regions where sliding occurs, the sliding portion of the ice flow is calculated from the SSA and the grounded from the SIA. Ice temperature is calculated through an enthalpy scheme for its thermodynamics [*Aschwanden et al.*, 2012], and a nondynamic basal hydrology where local melt will fill the till until it is saturated (2 m), all further melt will be lost.

A regional model domain has been developed by estimating the drainage basin of the Lamert-Amery glacial system by using the PISM drainage basin delineation tool (https://github.com/pism/regional-tools) and the BEDMAP2 surface elevation data [*Fretwell et al.*, 2013]. The drainage basin (Figure 1) is used within a square domain where the region outside the drainage basin is held at a constant thickness by modifying the surface mass balance to nullify the impact from the rest of Antarctica on the regional domain (-force_to_thickness PISM mechanism). The topography of the region is a combination of two data sets, with BEDMAP2 [*Fretwell et al.*, 2013] used beneath the grounded ice sheet and with RTOPO [*Timmermann et al.*, 2010] which incorporates *Galton-Fenzi et al.* [2008] under the floating ice. A 5 km region between the two data sets seaward of the grounding line was filled by linear interpolation. The surface mass balance and surface temperatures are the average fields 1979–2013 from RACMO2.3 ANT27/2 [*van Wessem et al.*, 2014]. The GHF data set is derived using the *Fox Maule et al.* [2005] methodology on the M7 magnetic field data. The basal melt parametrization for floating ice varies dependant on the depth of the ice and is derived from *Winkelmann et al.* [2011], with an additional scalar $\left(\frac{z}{1800}\right)^3$, which changes the distribution of melt to approximately replicate basal melt rates produced from an Amery Ice Shelf ocean cavity model [*Galton-Fenzi et al.*, 2012].

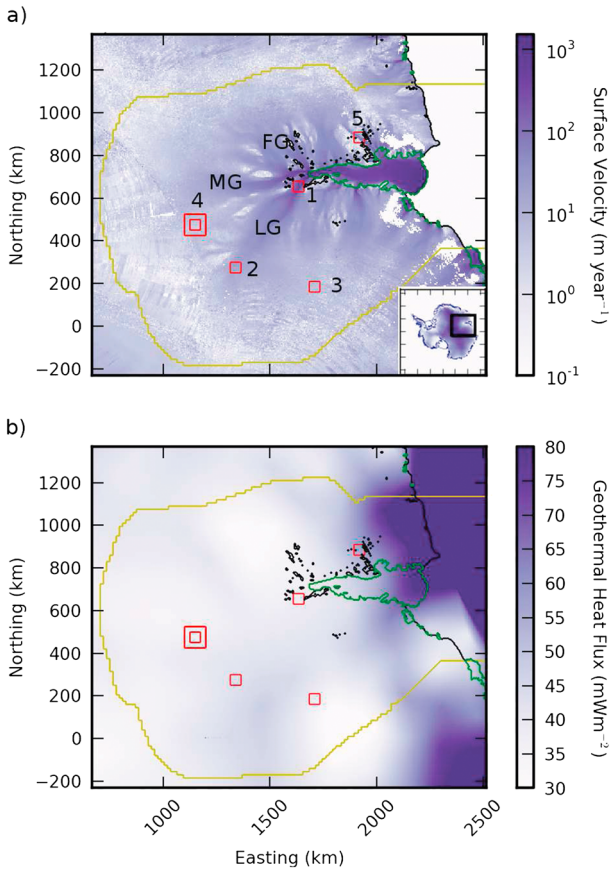

Figure 1. (a) The surface velocities of Lambert-Amery glacial system [*Rignot et al.*, 2011]. The inset indicates location within Antarctica. LG = Lambert Glacier, MG = Mellor Glacier, and FG = Fisher Glacier. (b) The background geothermal heat flux. The BEDMAP2 grounding line is indicated in green, the coastline and ice-free regions in black, the HHFR and associated experimental numbers are indicated in red (with Exp_4c the larger region at 4), and the force to thickness mask in yellow.

The regional model was optimized to minimize the difference between observed and modeled grounding line location, ice thickness, and surface velocity by testing a range of plausible values for the SIA and SSA enhancement factors, strength of the deformable till layer, and a variable within the pseudoplastic flow law (see the supporting information). The optimization process iteratively modified the set of parameters (see Tables S4 and S5), until a final set of parameters were found which best matched the observed system. These final parameters were used to initialize the model by running a non–mass-evolving model simulation with 10 km horizontal resolution and 15 m vertical resolution for 200,000 years until thermal equilibrium was reached. Once thermal equilibrium was reached, a simulation with 5 km horizontal resolution and 15 m vertical resolution was run until a steady state solution was achieved (approximately 5000 years). Our model solution is different to observations in the southern portion of the Amery Ice Shelf and adjacent grounded regions with slower velocities and increased thickness compared to observations (see Figure S1). In addition, there is less ice at high elevations toward the ice divides. These differences are attributed to a mixture of model resolution, overbuttressing of the ice shelf, and slightly high velocities at higher elevations shifting ice mass toward the grounding line. The velocities at the front of the ice shelf are lower than observations, with the lack of a pinning point on the northwestern front of the ice shelf leading to a wider and slower flow. The regional model solution is, however, considered realistic for the purpose of this study as we are investigating at the sensitivity of the grounded ice flow to a control model solution rather than observations.

3. Methods

A large portion of the Lambert-Amery glacial system is estimated to have a similar tectonic crustal history to the region in Prydz Bay that has been identified to contain HHFR [*Carson et al.*, 2014]. It is therefore plausible

Table 1. HHFR Differences for Thickness, Velocity, and Basal Temperature

	Ice Thickness (m)		Surface Velocity (m/yr)		Basal Temperature (K)	
Exp	Mean	Difference (%)	Mean	Difference (%)	Mean	Difference (K)
1	1993	0.03	257.7	−0.33	270.7	0.1
2	3100	−0.06	24.6	1.54	269.9	0.9
3	2686	−0.36	3.9	30.74	266.0	6.4
4a	1915	−0.84	2.8	52.84	261.0	8.9
5	965	−1.42	7.7	10.94	264.5	2.7
4b	1904	−1.42	3.7	100.2	265.4	13.3
4c	2200	−1.22	3.7	59.36	263.1	9.1

that HHFR will exist within the domain. To test the potential sensitivity of ice sheet flow to localized elevated geothermal heat flux, five regions were chosen to insert an idealized HHFR into the background field of the Lambert-Amery glacial system regional model. However, as we do not have any evidence to suggest specific locations, we perform five experiments, each representative of a different ice flow regimes (Figure 1): (1) Exp_1, fast ice stream flow region (≈250 m yr^{-1}); (2) Exp_2, slow ice stream flow region (≈ 25 m yr^{-1}); (3) Exp_3, region at high elevation with no delineated flow pathways; (4) Exp_4a, region between two glaciers (Lambert Glacier and Mellor Glacier); and (5) Exp_5, region terminated by a small outlet glacier.

The magnitude and size of the HHFR is representative of *Carson et al.* [2014], which showed GHF of 120 mW m^{-2} with horizontal extents ranging from 10 to 80 km. We include the HHFR anomalies by removing a 50 km × 50 km square of the background GHF for each of the five experiments, inserting a region of 25 km × 25 km with GHF equal to 120 mW m^{-2} and then use a cubic interpolation to smoothly transition from the idealized HHFR to the background GHF.

In addition, we supplement Exp_4a with two additional experiments: the importance of the magnitude and extent of the HHFR. Exp_4a was chosen as it provided the opportunity to investigate potential ice piracy between the two drainage basins and whether the ice is controlled by changes in the HHFR: (1) Exp_4b: elevated magnitude of the HHFR, 240 mW m^{-2}, and (2) Exp_4c: larger HHFR, removing a 100 km × 100 km square and inserting a 50 km × 50 km region with background GHF of 120 mW m^{-2}.

4. Sensitivity to Localized Regions of Elevated Geothermal Heat Flux

The ice velocity and thickness showed substantial change in three of the five ice flow regions (Table 1). The spatial changes in velocity (Figure 2) and thickness (Figure 3) show the effects of the HHFR impacting both upstream and downstream of the region.

Exp_1 showed minimal change to velocity, thickness, or basal temperature of the Lambert Glacier with the addition of the HHFR in the ice stream region of flow. The ice at the base of the ice sheet was at or close to melting before the HHFR was introduced, as velocities are in excess of 600 m yr^{-1} which will generate frictional and internal strain heating, and hence, the HHFR has limited effect on the velocities or thickness. The second region on the Lambert Glacier, Exp_2, showed acceleration at the edges of the flow but slower ice flow near the center of the HHFR and the ice flow, but overall, there was limited change in the velocity within the region and consequently, there was minimal change in ice thickness. These results are consistent with *Larour et al.* [2012] which found that regions of fast flow are not sensitive to GHF.

Exp_3 showed increased basal temperature and higher velocities in the HHFR with associated drops in the ice thickness. The velocity increase extended both downstream and upstream of the HHFR. What was previously a slow-moving region of no delineated flow now has a region of flow that is now moving faster than the surrounding ice. The flow adjacent to the stream-like flow is slower than the control. The mean basal temperature is still below melting point and no basal melt was produced.

When the HHFR is placed at the edge of the drainage basin (Exp_4a), the ice flow increased in a similar manner to that of Exp_3. There is evidence of the additional heat flowing along two separate pathways. The dominant pathway is toward the Lambert Glacier, but a visible increase can also be seen flowing toward the Mellor Glacier. This suggests that with the addition of the HHFR, more ice is flowing into the Lambert Glacier than before. The basal temperatures increased by 8.92 K, but the region is still well below pressure melting point.

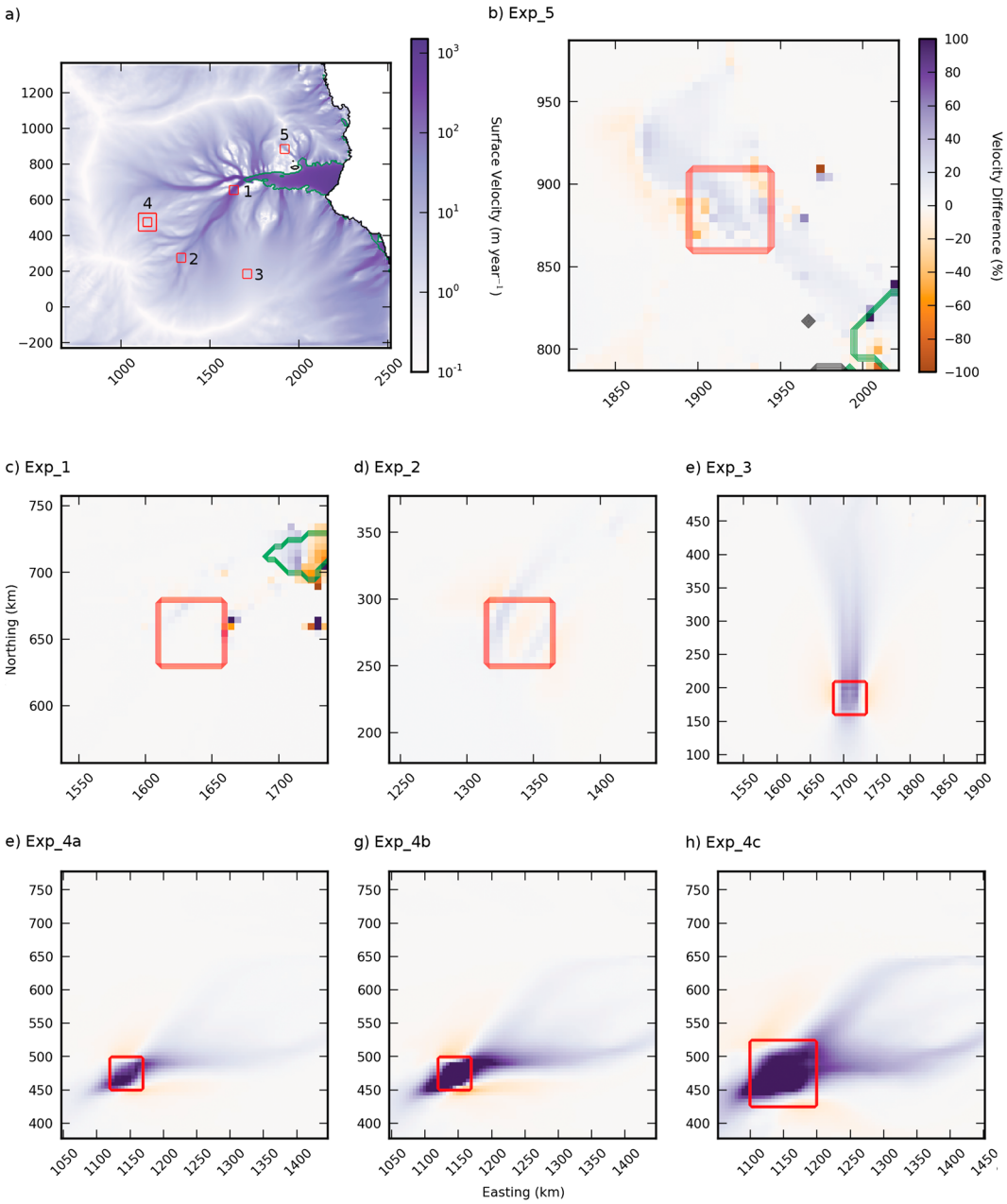

Figure 2. (a) Control surface velocity. Difference in surface velocity between control and (b) Exp_5, (c) Exp_1, (d) Exp_2, (e) Exp_3, (f) Exp_4a, (g) Exp_4b, and (h) Exp_4c. HHFR is indicated in red, grounding line in green, and coastline in black. The color bar on the top right applies to Figures 2b–2h.

The outlet glacier placement of the HHFR (Exp_5) showed faster velocities in the localized region along with changes in the ice thickness. The change in velocity is carried downstream, and as the mass flux through the glacier has increased, the ice margin has migrated inland as indicated by the change in velocity adjacent to the increase in flow. The basal temperature increased marginally.

Exp_4b shows increased basal temperature; however, melting point was still not quite reached with such high input. There was a small layer of temperate ice in the region, which suggests that it is nearing basal melting at some point within the HHFR. The velocity increased relative to Exp_4a, with a corresponding change in the local thickness. The enhanced velocity is transferred downstream, with more velocity heading down the west branch of the ice flow.

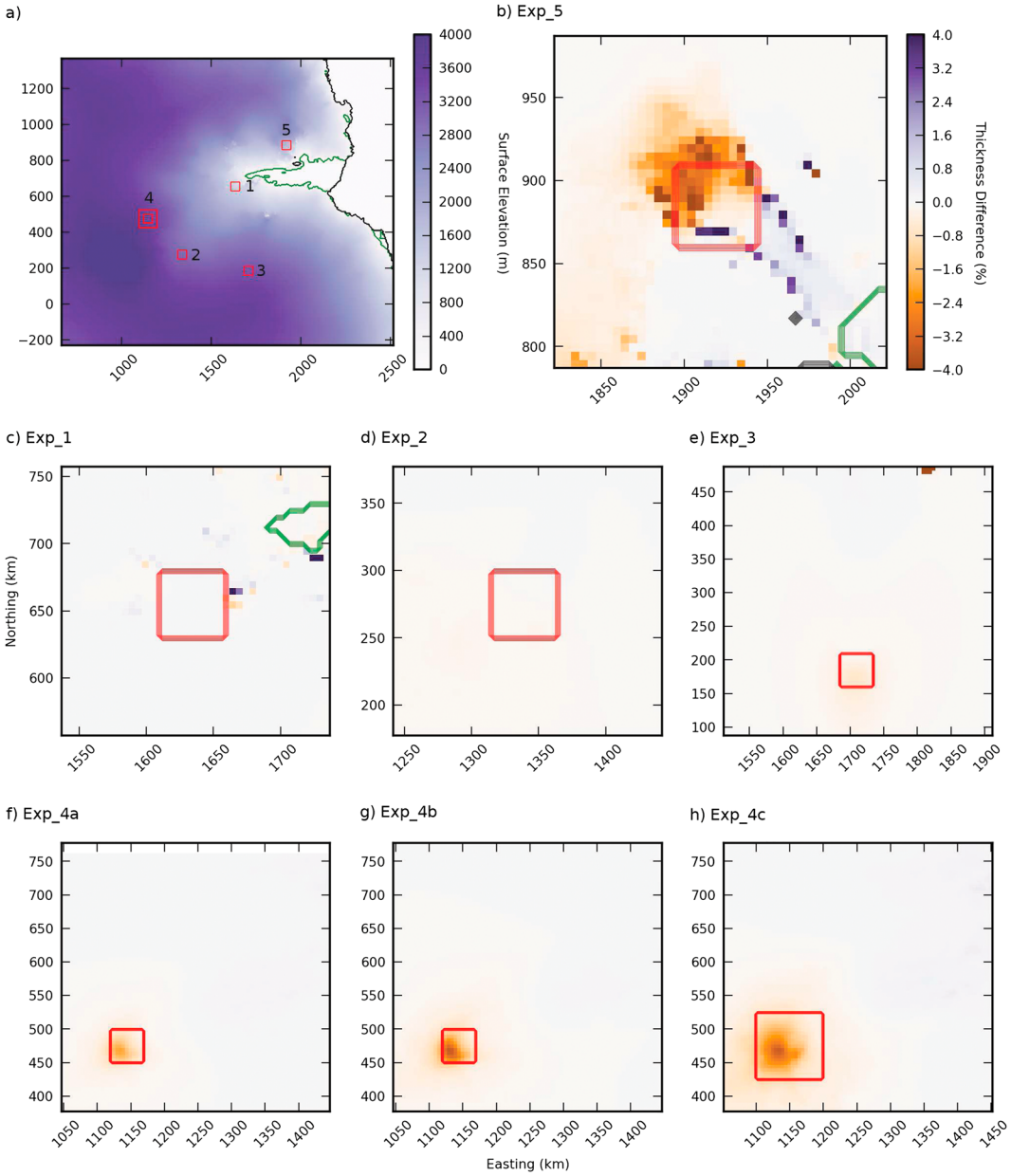

Figure 3. (a) Control surface elevation. Difference in surface elevation between control and (b) Exp_5, (c) Exp_1, (d) Exp_2, (e) Exp_3, (f) Exp_4a, (g) Exp_4b, and (h) Exp_4c. HHFR is indicated in red, grounding line in green, and coastline in black. The color bar on the top right applies to Figures 3b–3h.

When the region was doubled in size (Exp_4c), the basal temperature, surface velocity, and thickness changes are less pronounced than the Exp_4a; however, the spatial patterns are more pronounced. The local velocity increase is seen downstream, with the slowdown either side more pronounced. The spatial extent of the decrease in thickness is substantially larger relative to the HHFR than in other experiments. There is no evidence of basal melting, indicating that the increased flow is due to changes in the rheology of the ice and not due to basal lubrication.

5. Discussion

Comparison of outputs from an ice sheet model perturbed with HHFRs show that localized flow anomalies are important and aid in understanding areas of slow flow. In regions of low ice velocity, the addition of localized high GHF leads to a change in flow behavior, with the increase in ice velocity delineated from the surrounding

ice flow into a stream-like flow. The increased velocity is seen up to 100 km upstream and hundreds of kilometers downstream from the HHFR. The increase in velocity slows downstream to control values as the elevated ice temperature is diffused with distance. In the case of Exp_3, the diffusion continued approximately 300 km downstream of the 50 km wide HHFR. The basal temperatures were enhanced substantially within the HHFR; however, no basal melt was generated in any of the experiments. The upstream effect of the HHFR could indicate that the geothermal heat flux may be an important factor that is likely to influence the location of ice divides. HHFRs can influence ice flow pathways and may help explain current organization of ice flow, particularly where subglacial hydrological pathways may play a role. If a region has higher local GHF, it may preferentially flow along certain pathways, particularly combined with subglacial hydrology that may also enhance this effect. This is unlikely to be important on short time scales, but over millions of years combined with preferential erosion, a small difference in regional heat flow could contribute to the organization of ice flow. The current configuration of the present-day ice sheet will have already responded to HHFRs, with subglacial lakes at the onset of East Antarctic ice streams potentially caused by HHFR. This is supported by *Näslund et al.* [2005] who found that introducing variable regional heat flux in a Ferroscandian ice sheet model leads to faster ice flow, commensurate with findings from postglacial studies. We expect that as ice sheet models improve, the evidence of fine-scale variations in GHF will become more apparent.

The lack of basal melt in the HHFR was surprising, as the 120 mW m^{-2} and 240 mW m^{-2} GHF values are substantially more than the GHF calculated above subglacial lakes *Siegert* [2000]. This could be due to the GHF anomaly still being too low, with the 240 mW m^{-2} used still less than the 285 mW m^{-2} measured by *Fisher et al.* [2015] at a subglacial lake in West Antarctica. Alternatively, the regions chosen may had sufficient ice flow to advect heat downstream fast enough to stop basal melting. The subglacial lake mapping of this region suggests the existence of a lake somewhere between Exp_1 and Exp_2 [*Smith et al.*, 2009], which would be consistent with basal melt generated from frictional and strain heating as opposed to GHF. Subglacial lakes could be a fingerprint of regions of HHFR underneath the ice sheet, given that some of these subglacial lakes are found at the head of fast-flowing ice streams [*Bell et al.*, 2007]. It is possible that HHFRs are initiating ice flow through reduced friction as they flow over subglacial lakes in addition to the localized effect from enhanced viscosity due to warmer ice. There is dire need for further techniques for estimating the geothermal heat flux beneath the Antarctic ice sheet. Direct measurements would be ideal, but the logistical requirements for an Antarctic-wide validation make this an unrealistic aim, with targeted observations aimed to validate remote sensing techniques potentially a realistic goal.

GHF is an important boundary condition for determining the temperature profile throughout an ice sheet, but often, the selection of parameters for basal conditions overrides the difference GHF may have on the solution of an ice sheet model. Surface velocities of ice flow are our primary mechanism of evaluation of ice sheet models. The initiation of ice sheet models is reliant on an a priori surface velocity field derived from observations where the observational error is often similar or higher than the magnitude of the signal in slow-flowing regions. Improved resolution and accuracy of surface velocity measurements could identify regions of high heat flow in slow-flowing ice regions from their flow characteristics which would improve the initialization of ice sheet models. Often to obtain numerical solutions of ice sheets which match observed surface velocities, basal parameters which are the least observed components of the system are optimized or inverted for. If the region has faster flow due to higher GHF, it would be possible to erroneously simulate a match to observed surface velocities by using a softer till, for example. However, this could lead to other issues as ice temperature is transported downstream. In terms of our model and how this may possibly affect our results, we have used a relatively strong till resistance which may restrict the efficiency of possible feedbacks due to basal melting.

An alternative to altering a few parameters to match surface observations is basal inversions which provide a spatial distribution of key model variables [*Pattyn*, 2010]. These invert for the conditions at the bed based on surface velocity. Often these inversions include a viscosity term [*Morlighem et al.*, 2013], dependant on a temperature profile through the ice [*Gong et al.*, 2014]. These methods often have identified regions of sticky or slippery beds, but given that these are influenced by the estimated ice temperatures, they may be, in fact, identifying local-scale variations in the GHF. Regions of strong basal resistance may actually be colder ice, and regions of slippery bed may be regions of warmer ice. This could have ramifications for feedback mechanisms in ice models as regions inaccurately characterized as having slippery or sticky beds, or as being lubricated or frozen, will respond differently to accelerations in ice flow.

6. Conclusion

The inclusion of high heat flow regions caused by synthetic but plausible estimates of localized radiogenic crustal heat production caused local variation in ice velocity and consequently ice thickness. The largest influence was in regions of low ice velocity, with the impact seen 100 km upstream and 300 km downstream of the high heat flow region with a change in the flow behavior of the region. The flow changes from sheet flow to stream flow, with slight decreases in velocity seen adjacent to the region of stream-like flow. The increased local ice velocities will influence the organization of ice flow, which will affect long-period model runs. The direct influence on regions of fast flow is minimal, with heat generated by the fast flow dominating the local high heat flow, with no change in ice flow behavior. The existence of high heat flow regions may impact basal inversions for the initiation of ice sheet models by influencing the ice temperature and local viscosity of the ice. Further techniques to estimate or measure geothermal heat flux are required to fully assess possible impacts on ice dynamics and mass budget estimates.

Acknowledgments

This work was supported by the Australian Government's Cooperative Research Centres program through the Antarctic Climate and Ecosystems Cooperative Research Centre (ACE CRC). This research was supported under Australian Research Council's Special Research Initiative for Antarctic Gateway Partnership (Project ID SR140300001).This research was undertaken with the assistance of resources under projects m68 and gh8 from the National Computational Infrastructure (NCI), which is supported by the Australian Government. Development of PISM is supported by NASA grants NNX13AM16G and NNX13AK27G. The Geothermal Heat Flux data set updated using the MF7 magnetic field based on *Fox Maule et al.* [2005] was provided by Michael E. Purucker, NASA.

References

An, M., D. A. Wiens, Y. Zhao, M. Feng, A. Nyblade, M. Kanao, Y. Li, A. Maggi, and J.-J. Lévêque (2015), Temperature, lithosphere-asthenosphere boundary, and heat flux beneath the Antarctic Plate inferred from seismic velocities, *J. Geophys. Res. Solid Earth*, *120*, 8720–8742, doi:10.1002/2015JB011917.

Aschwanden, A., E. Bueler, C. Khroulev, and H. Blatter (2012), An enthalpy formulation for glaciers and ice sheets, *J. Glaciol.*, *58*(209), 441–457, doi:10.3189/2012JoGa11J088.

Bell, R. E., M. Studinger, C. A. Shuman, M. A. Fahnestock, and I. Joughin (2007), Large subglacial lakes in East Antarctica at the onset of fast-flowing ice streams, *Nature*, *445*, 904–907, doi:10.1038/nature05554.

Bueler, E., and J. Brown (2009), Shallow shelf approximation as a sliding law in a thermomechanically coupled ice sheet model, *J. Geophys. Res.*, *114*, F03008, doi:10.1029/2008JF001179.

Bueler, E., J. Brown, and C. Lingle (2007), Exact solutions to the thermomechanically coupled shallow-ice approximation: Effective tools for verification, *J. Glaciol.*, *53*, 499–516, doi:10.3189/002214307783258396.

Carson, C., and M. Pittard (2012), *A Reconaissance Crustal Heat Production Assessment of the Australian Antarctic Territory (AAT)*, Geoscience Australia, Canberra.

Carson, C. J., S. McLaren, J. L. Roberts, S. D. Boger, and D. D. Blankenship (2014), Hot rocks in a cold place: High sub-glacial heat flow in East Antarctica, *J. Geol. Soc.*, *171*(1), 9–12, doi:10.1144/jgs2013-030.

Fisher, A. T., K. D. Mankoff, S. M. Tulaczyk, S. W. Tyler, N. Foley, and the WISSARD Science Team (2015), High geothermal heat flux measured below the West Antarctic Ice Sheet, *Sci. Adv.*, *1*(6), e1500093, doi:10.1126/sciadv.1500093.

Fox Maule, C., M. E. Purucker, N. Olsen, and K. Mosegaard (2005), Heat flux anomalies in Antarctica revealed by satellite magnetic data, *Science*, *309*(5733), 464–467, doi:10.1126/science.1106888.

Fretwell, P., et al. (2013), Bedmap2: Improved ice bed, surface and thickness datasets for Antarctica, *Cryosphere*, *7*, 375–393, doi:10.5194/tc-7-375-2013.

Galton-Fenzi, B. K., C. Maraldi, R. Coleman, and J. Hunter (2008), The cavity under the Amery Ice Shelf, East Antarctica, *J. Glaciol.*, *54*, 881–887, doi:10.3189/002214308787779898.

Galton-Fenzi, B. K., J. R. Hunter, R. Coleman, S. J. Marsland, and R. C. Warner (2012), Modeling the basal melting and marine ice accretion of the Amery Ice Shelf, *J. Geophys. Res.*, *117*, C09031, doi:10.1029/2012JC008214.

Golledge, N. R., C. J. Fogwill, A. N. Mackintosh, and K. M. Buckley (2012), Dynamics of the Last Glacial Maximum Antarctic ice-sheet and its response to ocean forcing, *Proc. Natl. Acad. Sci.*, *109*, 16,052–16,056, doi:10.1073/pnas.1205385109.

Gong, Y., S. L. Cornford, and A. J. Payne (2014), Modelling the response of the Lambert Glacier-Amery ice shelf system, East Antarctica, to uncertain climate forcing over the 21st and 22nd centuries, *Cryosphere*, *8*(3), 1057–1068, doi:10.5194/tc-8-1057-2014.

Gooch, B. T., D. A. Young, and D. D. Blankenship (2016), Potential groundwater and heterogeneous heat source contributions to ice sheet dynamics in critical submarine basins of East Antarctica, *Geochem. Geophys. Geosyst.*, *17*, 395–409, doi:10.1002/2015GC006117.

King, M. A., R. Coleman, P. J. Morgan, and R. S. Hurd (2007), Velocity change of the Amery Ice Shelf, East Antarctica, during the period 1968–1999, *J. Geophys. Res.*, *112*, F01013, doi:10.1029/2006JF000609.

King, M. A., R. J. Bingham, P. Moore, P. L. Whitehouse, M. J. Bentley, and G. A. Milne (2012), Lower satellite-gravimetry estimates of Antarctic sea-level contribution, *Nature*, *491*, 586–589, doi:10.1038/nature11621.

Larour, E., M. Morlighem, H. Seroussi, J. Schiermeier, and E. Rignot (2012), Ice flow sensitivity to geothermal heat flux of Pine Island Glacier, Antarctica, *J. Geophys. Res.*, *117*, F04023, doi:10.1029/2012JF002371.

Martin, M. A., R. Winkelmann, M. Haseloff, T. Albrecht, E. Bueler, C. Khroulev, and A. Levermann (2011), The Potsdam Parallel Ice Sheet Model (PISM-PIK)—Part 2: Dynamic equilibrium simulation of the Antarctic ice sheet, *Cryosphere*, *5*, 727–740, doi:10.5194/tc-5-727-2011.

Morlighem, M., H. Seroussi, E. Larour, and E. Rignot (2013), Inversion of basal friction in Antarctica using exact and incomplete adjoints of a higher-order model, *J. Geophys. Res. Earth Surf.*, *118*, 1746–1753, doi:10.1002/jgrf.20125.

Näslund, J.-O., P. Jansson, J. L. Fastook, J. Johnson, and L. Andersson (2005), Detailed spatially distributed geothermal heat-flow data for modeling of basal temperatures and meltwater production beneath the Fennoscandian ice sheet, *Ann. Glaciol.*, *40*, 95–101, doi:10.3189/172756405781813582.

Pattyn, F. (2010), Antarctic subglacial conditions inferred from a hybrid ice sheet/ice stream model, *Earth Planet. Sci. Lett.*, *295*, 451–461, doi:10.1016/j.epsl.2010.04.025.

Pittard, M., J. Roberts, C. Watson, B. Galton-Fenzi, R. Warner, and R. Coleman (2015), Velocities of the Amery Ice Shelf's primary tributary glaciers, 2004–12, *Antarct. Sci.*, *27*, 511–523, doi:10.1017/S0954102015000231.

Rignot, E., J. Mouginot, and B. Scheuchl (2011), *MEaSUREs InSAR-Based Antarctica Ice Velocity Map [900m]*, National Snow and Ice Data Center, Boulder, Colo., doi:10.5067/MEASURES/CRYOSPHERE/nsidc-0484.001.

Sandiford, M., and S. McLaren (2002), Tectonic feedback and the ordering of heat producing elements within the continental lithosphere, *Earth Planet. Sci. Lett.*, *204*(1–2), 133–150, doi:10.1016/S0012-821X(02)00958-5.

Shapiro, N. M., and M. H. Ritzwoller (2004), Inferring surface heat flux distributions guided by a global seismic model: Particular application to Antarctica, *Earth Planet. Sci. Lett.*, *223*(1–2), 213–224, doi:10.1016/j.epsl.2004.04.011.

Siegert, M. J. (2000), Antarctic subglacial lakes, *Earth-Science Reviews*, *50*(1–2), 29–50, doi:10.1016/S0012-8252(99)00068-9.
Smith, B. E., H. A. Fricker, I. R. Joughin, and S. Tulaczyk (2009), An inventory of active subglacial lakes in Antarctica detected by ICESat (2003–2008), *J. Glaciol.*, *55*(192), 573–595, doi:10.3189/002214309789470879.
Timmermann, R., et al. (2010), A consistent data set of Antarctic ice sheet topography, cavity geometry, and global bathymetry, *Earth Syst. Sci. Data*, *2*(2), 261–273, doi:10.5194/essd-2-261-2010.
van Wessem, J. M., et al. (2014), Improved representation of East Antarctic surface mass balance in a regional atmospheric climate model, *J. Glaciol.*, *60*, 761–770, doi:10.3189/2014JoG14J051.
Wen, J., Y. Wang, W. Wang, K. C. Jezek, H. Liu, and I. Allison (2010), Basal melting and freezing under the Amery Ice Shelf, East Antarctica, *J. Glaciol.*, *56*, 81–90, doi:10.3189/002214310791190820.
Winkelmann, R., M. A. Martin, M. Haseloff, T. Albrecht, E. Bueler, C. Khroulev, and A. Levermann (2011), The Potsdam Parallel Ice Sheet Model (PISM-PIK)—Part 1: Model description, *Cryosphere*, *5*(3), 715–726, doi:10.5194/tc-5-715-2011.
Yu, J., H. Liu, K. C. Jezek, R. C. Warner, and J. Wen (2010), Analysis of velocity field, mass balance, and basal melt of the Lambert Glacier-Amery Ice Shelf system by incorporating Radarsat SAR interferometry and ICESat laser altimetry measurements, *J. Geophys. Res.*, *115*, B11102, doi:10.1029/2010JB007456.